Microwave damping in polycrystalline Fe-Ti-N films: Physical mechanisms and correlations with composition and structure

Sangita S. Kalarickal,[1] Pavol Krivosik,[1,2] Jaydip Das,[1] Kyoung Suk Kim,[3] and Carl E. Patton[1]
[1]*Department of Physics, Colorado State University, Fort Collins, Colorado 80523, USA*
[2]*Slovak University of Technology, 81219 Bratislava, Slovakia*
[3]*Deparment of Materials Science and Engineering, Korea University, Seoul 136-701, Korea*
(Received 30 October 2007; published 21 February 2008)

Ferromagnetic resonance (FMR) derivative linewidths were measured from 3 to 12 GHz on 50 nm thick sputtered polycrystalline Fe-Ti-N films with 3 at. % titanium and a nitrogen content (x_N) from 1.9 to 12.7 at. %. The measurements were made with both stripline and waveguide FMR spectrometers. Linewidths were generally lowest at x_N=7 at. %, with derivative linewidth (ΔH) values in the 15–25 Oe range and a nominally linear increase with frequency (f). This minimum linewidth composition is connected with the bcc to bct structural transition in the Fe-Ti-N system. Linewidths increased at both larger and smaller x_N values and were accompanied by the development of a more rounded frequency profile that is indicative of two-magnon scattering. All of the ΔH vs f data could be fitted successfully with a constant inhomogeneity broadening linewidth of 8–11 Oe, a two-magnon scattering (TMS) linewidth from the random grain-to-grain fluctuations in the effective anisotropy field directions for the polycrystal, and a magnon-electron (m-e) intrinsic relaxation term modeled through Gilbert damping with a single α value of 0.003. The actual fits were done through the convolution of a Gaussian linewidth for the inhomogeneity term and a Lorentzian linewidth for the TMS and m-e terms. The fitted anisotropy field parameters from the TMS analysis ranged between 398 and 883 Oe, with the minimum also at the bcc to bct structural transition at x_N=7 at. %.

DOI: 10.1103/PhysRevB.77.054427 PACS number(s): 76.50.+g, 75.50.Bb, 75.30.Ds

I. INTRODUCTION

Fe-*X*-N thin films, where *X* denotes Al, Ti, or Ta, for example, have been a subject of recent interest due to the large saturation magnetization, high initial permeability, and low coercive force in this system.[1–8] Nanocrystalline Fe-*X*-N alloy films, moreover, provide an attractive option for high frequency and high speed applications for microwave devices and information storage. While some important connections between film composition, crystal structure, microstructure, static magnetic properties, and magnetodynamic properties have been reported,[2,3,7–9] there are serious gaps in the understanding of the microwave loss.

The goal of the present work was to study the microwave damping properties in soft, polycrystalline Fe-Ti-N thin films as a function of frequency and nitrogen content. This work connects the change in structure and anisotropy with nitrogen to the magnetodynamics and, in particular, to the ferromagnetic resonance (FMR) linewidth. Specifically, the room temperature FMR response was measured as a function of frequency from 3 to 12 GHz for in-plane magnetized films with 3 at. % titanium and 1.9–12.7 at. % nitrogen. The line shapes show a more Gaussian than Lorentzian character at low frequency and a more Lorentzian than Gaussian character at high frequency. This observation leads to the use of a convolution approach to the overall linewidth analysis. The linewidth data were fitted to a combination of three processes: line broadening induced by inhomogeneities, two-magnon scattering due to randomly oriented grains in the polycrystal, and intrinsic Gilbert damping. The analysis indicates that these processes quantitatively define the overall loss picture and that two-magnon processes dominate. The extracted fit parameters correlate well with the expected structural changes with nitrogen content and static magnetic parameters.

The paper is organized as follows. Section II gives a brief review of past work on the Fe-Ti-N thin film system. Section III describes the thin film materials and gives details on the experimental setup. Section IV presents the experimental FMR linewidth results. This includes example absorption derivative profiles and Gaussian and Lorentzian best fits to these profiles, as well as data on linewidth vs frequency and nitrogen content. Section V considers line shapes and linewidths for inhomogeneous line broadening and *bona fide* relaxation processes, reviews the theoretical basis for the mechanisms of choice used here, and gives working equations for the linewidth analysis. Section VI presents theoretical fits to the data and discusses the different linewidth contributions as they relate to inhomogeneities, two-magnon scattering, and intrinsic losses. Section VII provides a summary and conclusion.

II. BRIEF NOTE ON STRUCTURE AND LINEWIDTH CONNECTIONS

Previous work on Fe-*X*-N alloy films has shown that there is a transition from a body centered cubic (bcc) structure to a body centered tetragonal (bct) structure at a nitrogen concentration (x_N) of about 7 at. %.[3,4,10,11] In a recent paper, Das *et al.*[12] have also established connections between the structural transition and a concomitant decrease in cubic anisotropy and increase in uniaxial anisotropy as the nitrogen level is increased. The operational anisotropy, cubic or uniaxial, is minimum at around 7 at. %.

While the above results, especially the data from Ref. 12, demonstrate the structural, crystallographic, and static mag-

TABLE I. Summary of parameters for the Fe-Ti-N films.

Nitrogen content x_N (at. %)	Grain size ξ (nm)	Saturation induction $4\pi M_s$ (kG)	FMR linewidth at 9.5 GHz ΔH (Oe)
1.9	20	19.0	76
3.9	15	18.8	57
5.4	10	18.2	46
7	8.5	16.8	27
8.4	7.5	15.3	27
12.7	4	13.9	32

netic property connections, similar links with dynamic properties are not yet clear. These systems do show relatively low FMR linewidths[9] that (1) decrease as x_N increases and (2) appear to correlate with the corresponding decrease in grain size. References 8 and 12 also suggest a possible connection between linewidth and magnetization ripple in thin films. The above cited FMR linewidth work, although somewhat limited, provides a natural lead into the present work. These results, described below, elucidate the connections between grain size, structural changes, and linewidth. To a large extent, these results also resolve the predominant two-magnon and inhomogeneity broadening contributions to the FMR linewidth in the Fe-Ti-N thin film system.

III. SAMPLE PROPERTIES AND FERROMAGNETIC RESONANCE MEASUREMENT TECHNIQUES

As with the work in Ref. 12, the polycrystalline Fe-Ti-N films were provided by C. Alexander, Jr. of the University of Alabama. The 50 nm thick films were prepared by dc magnetron sputtering on glass substrates. A dc magnetic field of about 300 Oe was applied in the plane of the substrates during sputtering to induce uniaxial anisotropy. All films had about 3 at. % Ti. The samples had x_N values of 1.9, 3.9, 5.4, 7.0, 8.4, and 12.7 at. %. The compositions were determined by x-ray photoelectron spectroscopy. The average grain size, as determined by transmission electron microscopy, ranged from 20 nm at x_N=1.9 at. % to about 4 nm at x_N =12.7 at. %. Preparation details are given in Ref. 2. A thorough discussion of the static magnetic properties and connections with structure is given in Ref. 12.

Table I lists key sample parameters. The x_N and grain size (ξ) values are from Ref. 2. The saturation induction ($4\pi M_s$) values are from Ref. 12. The listed 9.5 GHz FMR derivative linewidth (ΔH) values are from the present measurements. Note that saturation induction, grain size, and linewidth values generally decrease with increasing nitrogen content. This listing also demonstrates the relatively low ΔH values for the Fe-Ti-N film system.

Two systems were used for the linewidth measurements, a broadband stripline transmission spectrometer[13,14] for 2–7 GHz and a shorted waveguide reflection spectrometer[15,16] for 8–12 GHz. The FMR absorption derivative vs field profiles were generally undistorted. The FMR derivative linewidth, taken here as ΔH, was measured as the difference between the extrema of the FMR profile. The variation in these linewidths with frequency and nitrogen content, along with the analysis of these data in terms of basic loss and line broadening processes, is the focus of this work. It is to be emphasized that all experimental and theoretical linewidths presented here are given as derivative linewidths.

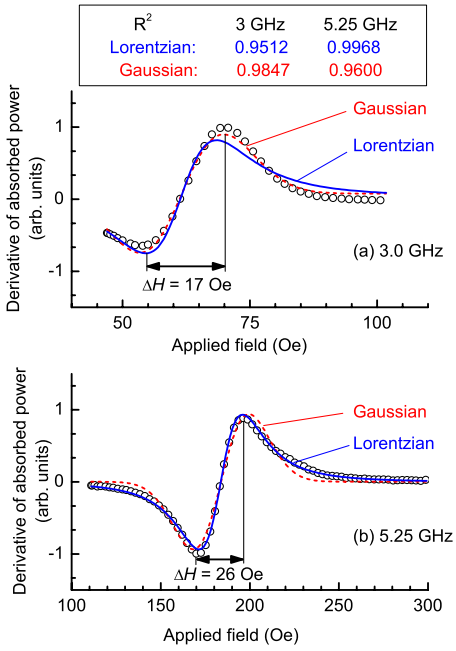

FIG. 1. (Color online) (a) and (b) show example ferromagnetic resonance absorption derivative vs field profiles for the film with x_N=5.4 at. % at 3.0 and 5.25 GHz, respectively. The dashed (red) and solid (blue) curves show Gaussian and Lorentzian fits to the data. The top table lists the regression parameters (R^2) for the four fits.

IV. FERROMAGNETIC RESONANCE LINEWIDTH RESULTS

Figure 1 shows example FMR absorption derivative profiles for the sample with x_N=5.4 at. % at 3.0 and 5.25 GHz. The open circles show the data. The dashed and solid curves, respectively, show Gaussian and Lorentzian derivative fits to the data. For this presentation, the standard regression parameter R^2 is used as a measure of the goodness of the fits. A perfect fit would correspond to R^2=1. These profiles demonstrate two things. First, one can see that the resonances are reasonably sharp and symmetric, with relatively narrow linewidths, as indicated. The second point concerns line shapes. One can see that for the 3.0 GHz data in Fig. 1(a), the Gaussian fit is better than the Lorentzian fit, and for the 5.25 GHz data in Fig. 1(b), the Lorentzian fit is better. While these differences are visible from the fits shown, the variation in the goodness of the fits shows up quite strongly in the listed R^2 values. These clear differences provide the motivation for

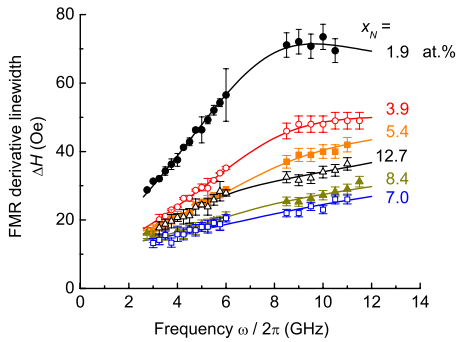

FIG. 2. (Color online) FMR derivative linewidth ΔH vs frequency $(\omega/2\pi)$ for all samples. The symbols show the data for different nitrogen contents, as indicated. The curves show model fits to the data based on the theoretical considerations discussed in the text.

the convolution approach to the linewidth analysis used below.

Figure 2 shows the FMR derivative linewidth ΔH as a function of frequency $(\omega/2\pi)$ for all samples. The symbols show the data for the different nitrogen levels, as indicated. The curves show fits to the data, based on theoretical considerations of two-magnon scattering, inhomogeneous line broadening, and intrinsic magnon-electron (m-e) scattering processes. The theory and fits are discussed in Secs. V and VI. Note that the frequency ω, specified in rad/s, plays an important role in the theoretical discussion to follow. The frequency parameter used for presentations of the data will usually be given in practical units as GHz.

There are two important points to be noted from Fig. 2. First, it is clear that the linewidth is not a linear function of frequency. While it is true that single crystal films and thin polycrystalline films can show a linear ΔH vs ω signature,[14,17–19] this cannot be taken as a general statement.[20–22] From the data, one can see that the response is closest to linear for an intermediate nitrogen level at $x_N \approx 7$ at. %. This composition also corresponds to the point where the linewidth is a minimum. As one goes below or above this level, one obtains larger linewidths and a more accentuated curved response. These effects are larger for x_N values below 7 at. % than for $x_N > 7$ at. %. Figure 3 shows the data of Fig. 2 in a ΔH vs x_N format for three selected frequencies, as indicated. In this format, the data demonstrate

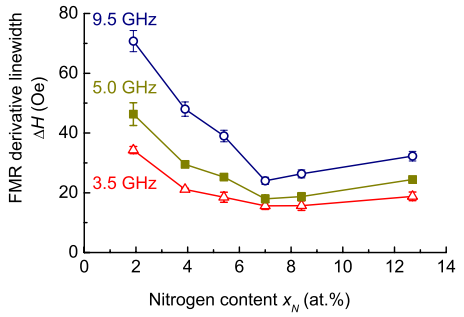

FIG. 3. (Color online) FMR derivative linewidth ΔH vs nitrogen content x_N at three selected frequencies, as indicated.

explicitly the linewidth minimum at $x_N \approx 7$ at. % and the more rapid rate of change for $x_N < 7$ at. % noted above.

The data shown in Figs. 2 and 3 can be understood in terms of the static magnetic and structural properties of the films. Inhomogeneous line broadening contributes a frequency and composition independent background linewidth. The linewidth minimum at $x_N \approx 7$ at. % is related to the established structural transition at this composition[3] and a minimum value for the overall magnetic anisotropy of the films.[12] The increases in linewidth above and below the $x_N \approx 7$ at. % point as well as the enhanced curvature of the ΔH vs ω response are due to two-magnon scattering (TMS).[23–26] These changes are related to the increase in anisotropy[12] and grain size changes. The remaining linewidth component follows the well established Gilbert (G) phenomenological model with a single, composition independent α value of 0.003. This α value is consistent with intrinsic magnon-electron scattering, the main intrinsic relaxation process for ferromagnetic resonance in metallic films.[27–30]

The next section provides an overview of these three linewidth mechanisms and develops working equations for fits to the data. Section VI presents the results of these fits and discusses the role of the different mechanisms.

V. LINEWIDTH MECHANISMS AND WORKING EQUATIONS

The most important point to note at the outset of this section is that inhomogeneities and physical loss processes lead to different line shapes, and one cannot simply add these two different types of linewidths to obtain a total linewidth. To lowest order, the effect of inhomogeneities amounts to the superposition of many local FMR absorption profiles with some spread in FMR fields that define the extent of the inhomogeneity. For random inhomogeneities, the spread will follow a Gaussian distribution. The corresponding FMR linewidth will, in the small signal limit, also have a Gaussian shape.

The other two processes, two-magnon scattering and intrinsic magnon-electron scattering, comprise physical relaxation mechanisms. In the small signal limit and to lowest order, these processes will have Lorentzian FMR absorption profiles. Because of this basic difference, any measured linewidth will be a convolution of the Gaussian profile associated with the inhomogeneous line broadening and the Lorentzian profile associated with the relaxation processes. This type of convolution applies, of course, only if these effects are independent of each other. The fits shown in Fig. 1 support the convolution argument. From the linewidth analysis in Sec. VI, it will be shown that the inhomogeneity linewidth contribution is larger than the linewidth associated with actual relaxation processes at lower frequencies, while the opposite is true at higher frequencies. This is precisely the indication from Fig. 1.

Based on the above, consider two contributions to the FMR linewidth. There is one linewidth associated with a Gaussian profile and related to inhomogeneity (INH) line broadening, termed ΔH_{INH}. In addition, there is a second linewidth, one associated with a Lorentzian (LOR) profile

and related to relaxation processes, termed ΔH_{LOR}. In the present situation, one can write, by way of approximation, $\Delta H_{\mathrm{LOR}}=\Delta H_{\mathrm{TMS}}+\Delta H_G$, where ΔH_{TMS} and ΔH_G denote the respective two-magnon scattering and magnon-electron or Gilbert contributions. Techniques for the convolution of Gaussian and Lorentzian line shapes and the use of Voigt functions are well established.[31] Here, however, the focus is on the linewidths, not on the overall shapes of the profiles. Working equations for the approximation of the derivative linewidths may be found in Ref. 31. The combined derivative linewidth ΔH takes the form

$$\Delta H \approx \frac{\Delta H_{\mathrm{INH}}^2 + 0.909\Delta H_{\mathrm{INH}}\Delta H_{\mathrm{LOR}} + 0.462\Delta H_{\mathrm{LOR}}^2}{\Delta H_{\mathrm{INH}} + 0.462\Delta H_{\mathrm{LOR}}}. \quad (1)$$

Note that Eq. (1) is specific to derivative linewidths. As the development below will show, the convolution of the inhomogeneous and Lorentzian contributions to the FMR response gives a good fit to the overall data. Figure 1 has already demonstrated the shift from Gaussian to Lorentzian line shapes as a function of frequency. Linewidth analyses based on a simple addition of ΔH_{LOR} and ΔH_{INH} are widely used.[18,21,32,33] Based on the remarks above, however, it is clear that convolution represents a more consistent approach when inhomogeneity and relaxation contributions to the linewidth are both present.

Now consider the individual contributions to the overall linewidth. As noted, line broadening due to inhomogeneities arises from the simple superposition of several local FMR profiles for different regions of the sample that are shifted in field because of some change in the magnetic properties. As one example, noninteracting regions with different M_s or anisotropy values can lead to such shifts. It is the assumed random distribution in these parameters relative to some mean value that gives rise to the overall Gaussian character of the line shape.

Inhomogeneous line broadening can take many forms. In polycrystalline ferrites with a random distribution of single crystal grains, for example, the line shape will map the random orientations of the crystallographic easy axes of the grains.[23] To lowest order, the corresponding spread in FMR fields will give a constant ΔH_{INH} that is independent of frequency. This model appears to apply to the present data. More complicated inhomogeneity line broadening models have also been proposed. These include a field dependent line broadening effect related to magnetization ripple.[9] A brief discussion of the ripple option will be given at the end of Sec. VI.

In addition to the conceptually simple Gaussian line broadening effects discussed above, inhomogeneities can also give rise to a Lorentzian linewidth contribution related to the scattering of spin waves that are at the same frequency as the driven FMR mode. The relaxation mechanism associated with this process is called two-magnon scattering. The process was discovered in the late 1950s and early 1960s in connection with FMR loss studies in bulk ferrites.[13,23,34,35] In this same time frame, TMS processes were also proposed as a possible linewidth mechanism in thin films.[13,36] In recent years, there has been a renewed interest in TMS processes in metallic ferromagnetic films, driven mainly by applications in high density and high speed magnetic recording.[21,24,37–40]

Briefly stated, TMS processes are related to short wavelength fluctuations in the local effective field in a given sample that break the orthogonality of the FMR mode and other degenerate spin wave modes. Examples can include the grain-to-grain fluctuations in the effective magnetocrystalline anisotropy field for a polycrystalline sample with randomly oriented grains, small pores or second phase material, and surface defects. Such fluctuations can lead to a coupling between the driven FMR mode and degenerate spin wave modes, and provide a channel for TMS relaxation. The corresponding linewidth will be strongly dependent on the density of states for degenerate spin wave modes and, hence, the shape of the spin wave band. The strongest coupling is usually for spin waves with wavelengths that are well above the size of the inhomogeneity. The process cuts off for wavelengths much shorter than the inhomogeneity size. For the 5–20 nm or so grain sizes applicable here, the cutoff will be for a spin wave wave number k on the order of 10^6–10^7 rad/cm. This is precisely the range of the available modes for the present Fe-Ti-N films at microwave frequencies.

The thin film TMS theory used here is based on the classical analysis developed in Ref. 24. References. 24 and 25 provide a qualitative introduction to thin film TMS processes in general, details on the theory, and working equations for practical calculations and fits to linewidth data. Brief comments are given below. Working equations for the linewidth calculations are given in the Appendix.

For a tractable analysis, one usually invokes the thin film approximation introduced by Harte,[41] in which the spin wave modes are taken to have no spatial variation over the film cross section. In this limit, the thin film TMS linewidth developed in Ref. 25 may be cast in the form

$$\Delta H_{\mathrm{TMS}} = \frac{1}{\sqrt{3}}\frac{|\gamma|H_A^2\xi^2}{P_A(\omega)}\int \Lambda_{0\mathbf{k}}C_{\mathbf{k}}(\xi)\,\delta(\omega-\omega_{\mathbf{k}})d^2k. \quad (2)$$

Here, H_A denotes an effective anisotropy field for the randomly oriented grains defined through $H_A=2K/M_s$, where K is an as yet unspecified anisotropy energy density for the material of interest. In Sec. VI, both cubic and uniaxial anisotropy contributions will be considered. The ξ parameter denotes the mean grain size. The $P_A(\omega)$ function is equal to $(\partial\omega_{\mathrm{FMR}}/\partial|\gamma|H)$ evaluated at $H=H_{\mathrm{FMR}}$, where ω_{FMR} is the field dependent FMR angular frequency and H_{FMR} is the resonance field at the operating frequency. The γ parameter denotes the gyromagnetic ratio. The P_A divisor in Eq. (2) accounts for the conversion between frequency and field swept linewidths.[14] The $C_{\mathbf{k}}(\xi)$ is the Fourier transform of the grain-to-grain dynamic internal field correlation function for the sample. Detailed considerations of $C_{\mathbf{k}}(\xi)$ based on the anisotropy in a system of randomly oriented grains are given in Ref. 25. This $C_{\mathbf{k}}(\xi)$ provides a specific form for the $\mathbf{k}$ dependence of the scattering for a given ξ value. The $\Lambda_{0\mathbf{k}}$ takes into account the averaging of the anisotropy axis fluctuations over the sample and the ellipticity of the precession response for both the uniform mode and the spin wave

modes. The integral folds in the scattering from the uniform mode to all available degenerate spin wave modes. The delta function $\delta(\omega-\omega_{\mathbf{k}})$ serves to select out these degenerate modes.

A full discussion of the dependences of the two-magnon linewidth on frequency, grain size, and other magnetic properties is beyond the scope of this paper. The key points for the present work are the following: (1) the different terms in Eq. (2) can lead to a complicated dependence of the two-magnon linewidth with frequency and grain size, and (2) the $\Delta H_{\mathrm{TMS}}(\omega)$ response is, in general, not linear. As shown in the next section, the explicit nonlinear $\Delta H_{\mathrm{TMS}}(\omega)$ response for these Fe-Ti-N films plays a crucial role in the explanation of the overall linewidth.

While two-magnon scattering is a physical relaxation process, it is based on the presence of inhomogeneities and can be taken as nonintrinsic. The last process needed for the present analysis is m-e scattering. This is the sole intrinsic relaxation process considered here. From the m-e consistent Gilbert model, one obtains a linewidth, taken here as ΔH_G, that takes the form

$$\Delta H_G = \frac{2}{\sqrt{3}}\frac{\alpha\omega}{|\gamma|}. \tag{3}$$

The linear increase in linewidth with frequency implicit in the Gilbert form has been widely observed in ferromagnetic metals.[14,19] As noted above, the Gilbert phenomenology is also consistent with the physical relaxation process of magnon-electron scattering. Recent ab initio band structure calculations of the m-e relaxation rates for iron, cobalt, and nickel give Gilbert damping α values that are consistent with the present results as well as with the other data cited above.[28] The $\sqrt{3}$ divisor in Eqs. (2) and (3) accounts for the conversion between a half-power linewidth and the derivative linewidth considered here, under the assumption of a Lorentzian absorption profile.

VI. LINEWIDTH ANALYSIS AND PHYSICAL CONNECTIONS

Section V reviewed the INH, TMS, and G contributions to the FMR linewidth, with an emphasis on the possible frequency dependences of these linewidth terms as they relate to the present data. This section presents explicit theoretical fits to the linewidth data from Sec. IV. The results provide a self-consistent explanation of the FMR linewidth for this series of Fe-Ti-N thin films. The overall fits are based on the convolution of the Gaussian inhomogeneity line broadening term with a combined Lorentzian term comprised of two-magnon scattering and magnon-electron relaxation. The correlation between the extracted TMS anisotropy scattering field parameter and composition provides particularly strong evidence for the importance of two magnon scattering in these films.

Figure 4 shows the ΔH vs frequency data from Fig. 2 for x_N=1.9 at. %, along with computed curves for the INH, TMS, and G linewidth contributions as well as the total fitted linewidth. The open circles denote the data; the dotted, dashed, and dot-dashed curves show the INH, TMS, and G linewidths, respectively; and the solid curve shows the total fitted linewidth. It was observed that fits with Gilbert α as a free parameter yielded the value of α for all samples as 0.003 ± 0.0002. The computed curves were obtained with the applicable parameter values from Table I and, as noted above, a free electron $|\gamma|/2\pi$ value of 2.8 GHz/kOe and a Gilbert α value of 0.003. Following Ref. 12, the anisotropy type for x_N=1.9 at. %, needed for the TMS $\Lambda_{0\mathbf{k}}$ function, was taken as cubic and the exchange energy parameter A was taken as 3×10^{-6} erg/cm. The ΔH_{INH} and H_A were taken as fitting parameters. The curves shown are for ΔH_{INH}=10 Oe and H_A=779.7 Oe. The regression parameter R^2 for the fit shown is 0.996.

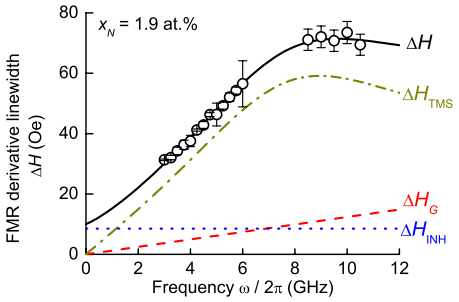

FIG. 4. (Color online) FMR derivative linewidth ΔH vs frequency $(\omega/2\pi)$ for x_N=1.9 at. %. The open circles show the data. The dotted (blue), dashed (red), and dot-dashed (green) lines show the computed inhomogeneity, Gilbert, and two-magnon scattering linewidth components, respectively. The solid (black) curve shows the combined linewidth according to Eq. (1).

Apart from the good theoretical fits, Fig. 4 shows three things. First, one can see that the convolution combines the three component linewidths to give an overall ΔH vs frequency response with a small upward curvature at low frequency. While this is clearly a small effect, it could turn out to be significant if the measurements could be extended to lower frequencies. This and related points will be considered at the end of the section.

The second point is that the dominant overall linewidth process, especially at the higher frequencies, is two-magnon scattering. The data and the fits show that this linewidth contribution has a somewhat complicated frequency dependence, with a linear increase at low frequency, a broad maximum of 8–10 GHz, and a small drop at higher frequencies. The signature of two-magnon scattering is very different from the simple linear response implicit in the Gilbert model. Based on the good fit shown here, it is clear that there can be no justification for the wide spread use of the Gilbert model to "explain" FMR linewidths in metallic films, often without any realistic consideration of the physical origins of these linewidths. The third point is that the fitted α value of 0.003 is consistent with expected values for m-e scattering in metallic films.[27–29]

Figure 5 shows all of the ΔH vs frequency data from Fig. 2, broken out into separate graphs for all the samples, along with curves for the overall linewidth fits. The open circles show the data and the solid curves show the fits. Apart from the previously noted common value of α (0.003) used for all

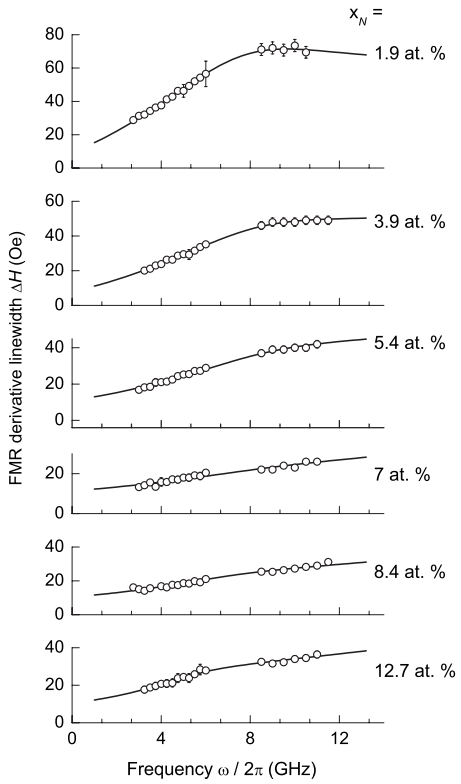

FIG. 5. FMR derivative linewidth ΔH vs frequency for all the samples. The solid curves give the calculations of the linewidth with the inhomogeneity line broadening, the two-magnon scattering, and the Gilbert damping contributions to the total linewidth.

fits, the curves in Fig. 5 are based on the parameters from Table I and the additional linewidth fitting parameters given in Table II. As with the data in Fig. 4, a constant background inhomogeneity linewidth ΔH_{INH} has been used for each graph, according to the values in Table II. Note that the exchange stiffness constant A was taken at 3×10^{-6} erg/cm for the films with $x_N \leqslant 7$ at. %,[12] and reduced to 2×10^{-6} and 1×10^{-6} erg/cm for the samples with x_N=8.4 and 12.7 at.%, respectively. In view of the bcc to bct structure change at $x_N \approx 7$ at.%, this change is reasonable.

One can also see from Table II that the fitted H_A values show a minimum at $x_N \approx 7$ at.% and then increase as one goes above or below this composition. Keep in mind that the

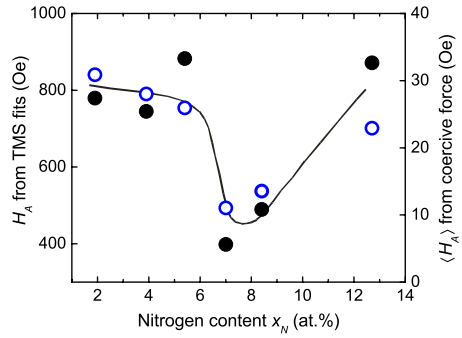

FIG. 6. (Color online) Anisotropy field parameter values as a function of the nitrogen content x_N. The solid (black) circles and left side axis show the H_A values from Table II. The error bars are on the order of the size of the points. The open (blue) circles and right side axis show the averaged anisotropy $\langle H_A \rangle$ values taken from Ref. 12. The solid curve serves as a guide for the eye for the trend of the data.

two-magnon fits are based on cubic anisotropy working equations for x_N values below 7 at.% and on uniaxial anisotropy for values of 7 at.% and above. This is indicated in the fifth column of Table II. These anisotropy details are significant for the discussion below.

The trend of the data with film composition was discussed in connection with Fig. 3. Here, the focus is on the trend of the fits with composition and the two-magnon scattering implications. Note that all of the fits are quite good. The regression R^2 values listed in Table II are all reasonably close to unity. The two-magnon part of the linewidth, mainly connected with the ΔH vs frequency dependences that deviate from a simple linear behavior, starts out large at x_N =1.9 at.%, initially drops off as x_N increases, is minimum for the x_N=7 and 8.4 at.% samples, and then becomes slightly larger as x_N moves toward 12.7 at.%.

The most important result from Fig. 5 and Table II relates to the minimum two-magnon linewidth contribution for x_N =7 at.% and the correlations with anisotropy and structural change. Figure 6 captures these results succinctly. The solid points show the H_A values as a function of x_N from Table II. The open circles show companion effective anisotropy data from Ref. 12. These latter data derive from coercive force measurements on these same samples and extractions of an effective cubic or uniaxial anisotropy energy density param-

TABLE II. Summary of fit parameters.

Nitrogen content x_N (at. %)	Inhomogeneity broadening ΔH_{INH} (Oe)	Exchange constant A ($\times10^{-6}$ erg/cm)	Anisotropy field H_A (Oe)	Anisotropy type	Fit regression R^2
1.9	10.0 ± 0.8	3.0	779.7 ± 4.0	Cubic	0.996
3.9	8.3 ± 0.5	3.0	745.1 ± 4.1	Cubic	0.997
5.4	11.0 ± 0.4	3.0	882.6 ± 8.6	Cubic	0.993
7	11.3 ± 0.5	3.0	398.4 ± 24.9	Uniaxial	0.939
8.4	10.5 ± 0.5	2.0	489.4 ± 13.7	Uniaxial	0.976
12.7	10.4 ± 0.7	1.0	871.6 ± 16.1	Uniaxial	0.982

eter, denoted here as a generic $\langle K \rangle$. The $\langle H_A \rangle$ values shown in the figure derive from an anisotropy connection of the form $\langle H_A \rangle = 2\langle K \rangle / M_s$. Following Ref. 12, and in the spirit of the two-magnon analysis here, the values for $x_N \leqslant 7$ at.% correspond to cubic anisotropy and those for $x_N > 7$ at% to uniaxial anisotropy. Note that the right side $\langle H_A \rangle$ scale in Fig. 6 differs from the left side H_A scale by a factor of 30–80. This difference in scale is discussed in Ref. 12. The curve through the ensemble of data points is intended as a guide for the eye.

Figure 6 makes explicit the minimum in the H_A values from the two magnon fits at $x_N \approx 7$ at.%. It also demonstrates the consistency between these data and the averaged $\langle H_A \rangle$ results from Ref. 12. These results, in combination with the good match between experiment and theory in Fig. 5, provide convincing arguments for (1) a strong composition dependent two-magnon contribution to the linewidth, (2) clear correlations with a structure change at $x_N \approx 7$ at.%, and (3) quantitative fits that support the use of a bcc model below and a bct model above the transition point. As one such quantitative point of comparison, the cubic anisotropy energy density parameter from the TMS fit for $x_N \approx 1.9$ at% is obtained as 590×10^3 erg/cm^3. The literature value for pure iron is about 480×10^3 erg/cm^3.[42]

Up to now, there has been no comment on the role of grain size on the calculated TMS linewidth. As evident from Eq. (2), the grain size ξ enters the TMS analysis both as a prefactor and as a parameter inside the correlation integral. The grain size, however, was not taken as a fitting parameter. All of the fits were based on the measured grain sizes from Ref. 12, as listed in Table I. It turns out that any small change in grain size from these measured values causes a significant degradation in the best fit matchup with the data. This means, in turn, that the "best fit" ξ value matches up nearly perfectly with the measured grain size. This lends additional credence to the two magnon linewidth results presented above.

As noted in Sec. V, a field dependent inhomogeneity line broadening mechanism related to magnetization ripple has also been proposed. Reasonable fits to the present data could also be obtained from this model, the working equations in Ref. 9, and the averaged effective uniaxial anisotropy field determinations from Ref. 12. With this approach, the R^2 values for fits based on a ripple inhomogeneity line broadening are about the same as those in Table II for a constant ΔH_{INH}. From these results, one could argue that magnetization ripple is a reasonable source of the ΔH_{INH}. Such a mechanism can be justified here because ripple line broadening has a very weak dependence on the applied field in the FMR regime of fields and frequencies studied here. On the other hand, the ripple model also predicts a very rapid increase in the inhomogeneity linewidth at frequencies below 2 GHz. Up to now, there is no evidence for such a response at low frequency.

VII. SUMMARY AND CONCLUSION

In summary, the above sections have described 3–12 GHz ferromagnetic resonance linewidth measurements and analyses for a series of polycrystalline Fe-Ti-N films with nitrogen concentrations (x_N) ranging from 1.9–12.7 at.%. The data show clear departures from the linear linewidth vs frequency response that is usually taken as the norm for metallic films. The linewidths generally show a minimum at the bcc to bct structural transition point at $x_N \approx 7$ at.%.

A model with three terms, a constant inhomogeneous broadening linewidth, a two-magnon scattering linewidth term, and an intrinsic magnon-electron term modeled through a Gilbert damping form, gives good fits to the data. The particular fits obtained here were based on the convolution of a Gaussian form for the inhomogeneous term and a Lorentzian for the two remaining physical processes. The fitted two-magnon term gives values of the effective anisotropy field in the grains that are consistent with previous reports and correlate with the structural transition noted above.

TABLE III. Averaging coefficients for the variation in the anisotropy direction.

	Averaging coefficients			
Type of anisotropy	c_1	c_2	c_3	c_4
In-plane uniaxial	1/8	3/32	0	1/8
First order cubic	29/420	29/420	3/140	1/105

ACKNOWLEDGMENTS

This work was supported in part by the Office of Naval Research (USA) Grant No. N00014-06-1-0889, the U.S. Army Research Office, MURI Grant No. W911NF-04-1-0247, the Information Storage Industry Consortium (INSIC) Extremely High Density Recording (EHDR) program, and Seagate Technologies. The samples and the grain size analysis were provided by J. C. Alexander, Jr., MINT Center, University of Alabama.

APPENDIX

This appendix gives working equations for the evaluation of the terms in Eq. (2) for the two-magnon scattering field swept linewidth ΔH_{TMS}. These equations are specific to an in-plane magnetized thin film with an average grain size ξ, taken here to be the same as the correlation length for the grain-to-grain fluctuation in the effective anisotropy field. All of the applicable parameters have been defined in the discussion of Eq. (2). For readability, some of these definitions are repeated below.

The Fourier transform of the grain-to-grain effective field correlation function, $C_{\mathbf{k}}(\xi)$, is taken to have the form

$$C_{\mathbf{k}}(\xi) = \frac{1}{[1 + (k\xi)^2]^{3/2}}, \tag{A1}$$

where $k = |\mathbf{k}|$ is the spin wave wave number. In real space, this corresponds to a point-to-point effective field correlation

that falls off as $e^{-|\mathbf{r}-\mathbf{r}'|/\xi}$, where $\mathbf{r}$ and $\mathbf{r}'$ represent two separate positions in the film.[24]

The ellipticity function $\Lambda_{0\mathbf{k}}$ is given by

$$\Lambda_{0\mathbf{k}} = c_1 e_0 e_{\mathbf{k}} + \frac{c_2}{e_0 e_{\mathbf{k}}} + c_3\left(\frac{e_0}{e_{\mathbf{k}}} + \frac{e_{\mathbf{k}}}{e_0}\right) + c_4. \tag{A2}$$

Here, e_0 and $e_{\mathbf{k}}$ denote the ellipticity of the uniform mode and a given spin wave mode at wave vector $\mathbf{k}$, respectively. These ellipticity factors are given by

$$e_0 = \sqrt{\frac{H + 4\pi M_s}{H}} \tag{A3}$$

and

$$e_{\mathbf{k}} = \sqrt{\frac{H + Dk^2 + 4\pi M_s N_k}{H + Dk^2 + 4\pi M_s (1 - N_k)\sin^2\theta_k}}, \tag{A4}$$

where D is an exchange field parameter related to the exchange energy parameter A according to $D = 2A/M_s$. The thin film dipole field effective demagnetizing factor N_k is given by $N_k = (1 - e^{-kd})/kd$, where d is the film thickness,[41] and θ_k is the angle between the in-plane static field direction and the in-plane wave vector $\mathbf{k}$ direction. The c_1, c_2, c_3, and c_4 parameters are connected to averages of the scattering over all of the randomly oriented grains.[24] The numerical values of these parameters for cubic and uniaxial anisotropies are listed in Table III. Finally, the $P_A(\omega)$ function in Eq. (2) is given by

$$P_A(\omega) = \sqrt{1 + \left(\frac{4\pi M_s}{2\omega/\gamma}\right)^2}. \tag{A5}$$

[1] D. J. Rogers, S. Wang, D. E. Laughin, and M. H. Kryder, IEEE Trans. Magn. **28**, 2418 (1992).
[2] Y. Ding and J. C. Alexander, J. Appl. Phys. **91**, 7833 (2002).
[3] Y. Ding, S. C. Byeon, and J. C. Alexander, IEEE Trans. Magn. **37**, 1776 (2001).
[4] Y. Ding and J. C. Alexander, IEEE Trans. Magn. **42**, 5 (2006).
[5] A. Chakraborty, K. R. Mountfield, G. H. Bellesis, D. N. Lambeth, and M. H. Kryder, J. Appl. Phys. **80**, 1012 (1996).
[6] B. Viala, M. K. Minor, and J. A. Barnard, J. Appl. Phys. **80**, 3941 (1996).
[7] S. C. Byeon, Y. Ding, and C. Alexander, Jr., IEEE Trans. Magn. **36**, 2502 (2000).
[8] J. Rantschler, Ph.D. thesis, University of Alabama, 2003.
[9] J. Rantschler and C. Alexander, J. Appl. Phys. **93**, 6665 (2003).
[10] A. V. Mijiritskii and D. O. Boerma, Phys. Rev. B **64**, 035410 (2001).
[11] J. M. D. Coey and P. A. I. Smith, J. Magn. Magn. Mater. **200**, 405 (1999).
[12] J. Das, S. S. Kalarickal, K. S. Kim, and C. E. Patton, Phys. Rev. B **75**, 094435 (2007).
[13] C. E. Patton, J. Appl. Phys. **39**, 3060 (1968).
[14] S. S. Kalarickal, P. Krivosik, M. Wu, C. E. Patton, M. L. Schneider, P. Kabos, T. J. Silva, and J. P. Nibarger, J. Appl. Phys. **99**, 093909 (2006).
[15] M. J. Hurben, Ph.D. thesis, Colorado State University, 1996.
[16] J. J. Green and T. Kohane, Semicond. Prod. Solid State Technol. **7**, 46 (1964).
[17] C. E. Patton, Z. Frait, and C. H. Wilts, J. Appl. Phys. **46**, 5002 (1975).
[18] B. Heinrich, J. F. Cochran, and R. Hasegawa, J. Appl. Phys. **57**, 3690 (1985).
[19] B. Heinrich, R. Urban, and G. Waltersdorf, J. Appl. Phys. **91**, 7523 (2002).
[20] J. Lindner, K. Lenz, E. Kosubek, K. Baberschke, D. Spoddig, R. Meckenstock, J. Pelzl, Z. Frait, and D. Mills, Phys. Rev. B **68**, 060102 (2003).
[21] K. Lenz, H. Wende, W. Kuch, K. Baberschke, K. Nagy, and A. Janossy, Phys. Rev. B **73**, 144424 (2006).
[22] K. Zakeri, J. Lindner, I. Barsukov, R. Meckenstock, M. Farle, U. von Hörsten, H. Wende, W. Keune, J. Rocker, S. S. Kalarickal, K. Lenz, W. Kuch, K. Baberschke, and Z. Frait, Phys. Rev. B **76**, 104416 (2007).
[23] E. Schloemann, J. Phys. Chem. Solids **6**, 242 (1958).
[24] R. McMichael and P. Krivosik, IEEE Trans. Magn. **40**, 2 (2004).
[25] P. Krivosik, N. Mo, S. S. Kalarickal, and C. E. Patton, J. Appl. Phys. **101**, 083901 (2007).
[26] M. Sparks, *Ferromagnetic Relaxation Theory* (McGraw-Hill, New York, 1964).
[27] B. Kuanr, R. Camley, and Z. Celinski, J. Appl. Phys. **95**, 6610 (2004).
[28] K. Gilmore, Y. U. Idzerda, and M. D. Stiles, Phys. Rev. Lett. **99**, 027204 (2007).
[29] C. Scheck, L. Cheng, and W. E. Bailey, Appl. Phys. Lett. **88**, 252510 (2006).
[30] V. Kamberský and C. E. Patton, Phys. Rev. B **11**, 2668 (1975).
[31] A. M. Stoneham, J. Phys. D **5**, 672 (1972).
[32] B. Kuanr, R. Camley, and Z. Celinski, J. Magn. Magn. Mater. **286**, 276 (2005).
[33] S. Mizukami, Y. Ando, and T. Miyazaki, Phys. Rev. B **66**, 104413 (2002).
[34] C. E. Patton, C. H. Wilts, and F. B. Humphrey, J. Appl. Phys. **38**, 1358 (1967).
[35] E. Schloemann, AIEE Special Publication No. T-91, 1956 (unpublished), p. 600.
[36] A. J. Bertaud and H. Pascard, J. Appl. Phys. **36**, 970 (1965).
[37] R. Arias and D. L. Mills, Phys. Rev. B **60**, 7395 (1999).
[38] R. McMichael, M. Stiles, P. Chen, and W. Egelhoff, Jr., J. Appl. Phys. **83**, 7037 (1998).
[39] A. Y. Dobin and R. H. Victoria, Phys. Rev. Lett. **92**, 257204 (2004).
[40] G. Woltersdorf and B. Heinrich, Phys. Rev. B **69**, 184417 (2004).
[41] K. J. Harte, J. Appl. Phys. **36**, 960 (1965).
[42] G. Herzer, IEEE Trans. Magn. **26**, 1397 (1990).